



SPE 36651

## Reservoir Fracture Mapping Using Microearthquakes: Two Oilfield Case Studies

W.S. Phillips, J.T. Rutledge, SPE, and T.D. Fairbanks, Nambe Geophysical Inc, T.L. Gardner SPE and M.E. Miller, Exxon USA and B.S. Maher, Los Alamos National Laboratory

Copyright 1998, Society of Petroleum Engineers, Inc.

Electronic reproduction, distribution, or storage of any part of this paper for commercial purposes without the written consent of the Society of Petroleum Engineers is prohibited. Permission to copy is restricted to an abstract of not more than 300 words; illustrations may not be copied. The abstract must contain conspicuous acknowledgment of where and by whom the paper was presented. Write Librarian, SPE, P.O. Box 833836, Richardson, TX 75083-3836, U.S.A., fax 01-972-952-9435.

### Abstract

Patterns of microearthquakes detected downhole defined fracture orientation and extent in the Austin chalk, Giddings field, Texas and in the 76 field, Clinton County, Kentucky. We collected over 480 and 770 microearthquakes during hydraulic stimulation at two sites in the Austin chalk, and over 3200 during primary production in Clinton County. Data were of high enough quality that 20%, 31% and 53% of the events could be located, respectively.

Reflected wave data constrained microearthquakes to the stimulated depths at the base of the Austin chalk. In plan view, microearthquakes defined elongate fracture zones extending from the stimulation wells parallel to the regional fracture trend. However, widths of the stimulated zones differed by a factor of five between the two Austin chalk sites, suggesting a large difference in the population of ancillary fractures. Post-stimulation production was much higher from the wider zone.

At Clinton County, microearthquakes defined low-angle, reverse-fault fracture zones above and below a producing zone. Associations with depleted production intervals indicated the mapped fractures had been previously drained. Drilling showed that the fractures currently contain brine. The seismic behavior was consistent with stress changes associated with poroelastic effects above and below a drained volume or with the mass exchange of brine replacing produced oil.

### Introduction

Microearthquakes often accompany reservoir stimulation and production. By collecting high-quality seismic data, the microearthquakes can be mapped, yielding potentially extensive and high-resolution information

about the fracture system. Fracture maps may be useful in planning infill and horizontal drilling, and in designing and evaluating hydraulic stimulation and enhanced recovery operations in fracture-dominated oil and gas reservoirs.

Borehole geophones at reservoir depths provide the high-quality data needed to determine microearthquake location patterns. But when special observation wells must be drilled, microseismic studies can be expensive. To demonstrate that high-quality data can be collected inexpensively, we deployed geophones in existing wells and developed techniques for analyzing data from the resulting, sparse array of instruments. We hope the demonstration of inexpensive and effective methods will result in the routine application of microearthquake techniques to study reservoir fracture systems.

Methods currently applied to study fracture systems include tilt-meter surveys that give gross fracture characteristics<sup>1,2</sup>, and borehole optical, acoustic or resistivity (formation microscanner) surveys that give detailed information along the borehole<sup>3</sup>. More specialized methods include shear shadowing<sup>4,7</sup>, coring or mineback experiments<sup>8,9</sup> and anisotropy from surface seismic<sup>10</sup>. While less detailed than borehole surveys, less convenient than surface measurements such as tiltmeter or seismic, and less directly interpretable than coring studies, the microseismic technique provides a combination of resolution, coverage and economy that is difficult to surpass with other methods.

Downhole microseismic monitoring has been applied successfully to hydraulic-stimulation experiments in hot-dry-rock geothermal reservoirs at Fenton Hill, New Mexico<sup>11-13</sup>, the U.K.<sup>14,15</sup>, Japan<sup>16</sup> and France<sup>17</sup>. Tomography has been performed using these data indicating low-velocity process zones in the seismic region<sup>18</sup>. Additional data processing defined planar features that represent individual joints that slipped<sup>19-21</sup>. These experiments took place in hard, crystalline rock, through which elastic waves propagate efficiently. In spite of poorer wave-propagation properties, stimulation-related microearthquakes have been successfully mapped in sedimentary environments using downhole

geophones or accelerometers<sup>22-29</sup>. Production-related microearthquakes have been studied for years<sup>30-33</sup>, most work done using surface geophones.

In the following, we will describe remote well microseismic monitoring in the Austin chalk, Giddings field, Texas (**Fig. 1**) and the 76 field, Clinton County, Kentucky (**Fig. 2**). Microearthquakes were associated with hydraulic stimulation in the Austin chalk, and with primary production in Clinton County. We monitored from existing wells to demonstrate the economy of the technique. These deployments began as reconnaissance experiments. However, the data were of such quality to allow accurate mapping of the microearthquake data, yielding previously unknown details of the reservoir fracture systems.

## Setting

**Austin Chalk.** The Giddings field was discovered in 1960 by Union Producing Company with the drilling of the Pruess No. 1 well immediately west of the town of Giddings in Lee County, Texas. The field now covers portions of Lee, Burleson, Bastrop, Fayette, Brazos, and Washington Counties. Cumulative production from the Giddings field is over 60 million m<sup>3</sup> (380 million bbl) oil and 60 billion m<sup>3</sup> (2.1 trillion ft<sup>3</sup>) gas. In the Giddings field, 98% of the oil has been produced from the Austin chalk.

The Austin chalk is a fractured limestone with a matrix porosity of 10% and matrix permeability of 0.01 to 0.1 millidarcys. The presence of fractures in the Austin chalk at Giddings field is due to the bending of this brittle limestone over a deeper and older Jurassic shelf margin or hinge line, trending northeast-southwest, roughly parallel to the Gulf coast. These fractures enable the Austin chalk to produce at relatively high rates (160 m<sup>3</sup> or 1000 bbl per day) and reach single well maximum cumulative production approaching 80,000 m<sup>3</sup> (500,000 bbl) of oil. Recovery efficiency for the Austin Chalk at Giddings is thought to be on the order of 7-10% of the original oil in place.

In the Austin chalk, hydraulic stimulation is used to complete new wells and to enhance production from older wells. During stimulation, the water forced into untapped areas of the chalk is thought to replace, and thus mobilize hydrocarbons residing in small cracks through imbibition. To study the stimulated fracture system, we monitored microseismicity during two, 4000 m<sup>3</sup> (25,000 bbl) stimulations of the Austin chalk (peak pressure 21 MPa, 3000 psi; peak flow rate 13 m<sup>3</sup>/minute, 80 bbl/minute) that included acid and diverter (rock salt) phases.

**Clinton Co.** Clinton County is located within the Cumberland Saddle of the Cincinnati Arch, immediately west of the Grenville Front. Oil is produced from low porosity (<2%) carbonate rocks of Ordovician age, spanning the section from the Lexington Limestone to the Knox Group, at depths from 230 to 730 m. Fracture storage and permeability is suggested by isolated, high-volume production wells. Initial production rates as high as 64 m<sup>3</sup> (400 bbl) per hour and cumulative production of 16,000 m<sup>3</sup> (100,000 bbl) from a single well have been reported<sup>34</sup>.

Basement-controlled wrench-fault structures have been associated with oil production from shallow (135 to 180 m), carbonate reservoirs, 65 km west of Clinton County<sup>35</sup>. Local operators have also based recent drilling programs on fracture/lineament patterns delineated on side-looking airborne radar images and interpreted to be associated with right-lateral wrenching of an east-west trending basement fault. In general, only near-vertical fracture sets have been considered in these models. We deployed geophones in Clinton Co. wells to delineate the reservoir fracture systems. Results of two, earlier tests have been presented<sup>36</sup>; here we summarize results of our latest, and most seismically active deployment.

## Data

We collected microseismic data using downhole, 3-component geophone tools. A mechanical arm coupled the instruments to the borehole wall. The tools were equipped with 8- or 30-Hz geophones. Downhole amplification of the geophone outputs was 60 dB. At the surface, the data signals were further amplified and anti-alias filtered before input to a digital, PC-based, event-detection system<sup>37</sup>. Data were sampled at 5 KHz. Events from both sites contained clear compressional (P) and shear (S) phases. S-to-P amplitude ratios were similar to those of tectonic earthquakes and initial P-wave motions were toward the source for some events and away for others, indicating predominantly shear-slip, rather than tensile, source mechanisms.

**Austin Chalk.** We deployed downhole geophones at two sites in the Giddings field (**Fig. 1**). We monitored from well CPU 1-2 near Cook's Point, depth 2097 m, 9/91 to 11/91, and from wells Matcek 4 and 3 near Caldwell, depths 2259 m and 2280 m, 11/91 to 9/92 and 5/92 to 9/92, respectively. Wells were prepared by removing production tubing, setting temporary bridge plugs just above the perforated interval and filling with non-corrosive fluid.

Over 480 and 770 microearthquakes were collected during stimulations of wells CPU 2-2 and Matcek 1,

respectively. At both sites, seismicity started within one hour of the pumping and decayed away after final shut-in (**Fig. 3**). Signal energy peaked between 200 and 500 Hz (**Fig. 4**). Horizontally polarized S waves arrived earlier than vertically polarized S waves, suggesting bedding-related anisotropy. This effect required us to rotate horizontal-component seismograms to radial and transverse directions with respect to the incident raypath to determine S-wave arrival times in a consistent manner. The raypath directions were estimated using the initial motion in the horizontal plane (hodogram) of the P-waves. S-wave reflections off the high-contrast Eagleford-Buda boundary below the Austin chalk arrive after the S waves in many records (**Fig. 4**). These reflections became important for determining event depths. Perforation shots fired at both injection points produced good-quality records and helped to calibrate velocities and geophone orientations.

**Clinton Co.** We deployed two geophones in well GT8 at depths of 427 and 244 m, 1/95 to 8/95. A third geophone was placed in well BU1 at a depth of 396 m, 3/95 to 8/95 (**Fig. 2**).

Monitoring began 6 weeks after initial production from well HT1 (**Fig. 5**). The production-rate decrease at week 13 was followed by an event-rate decrease at week 15. We presume production declined after week 22, but records were not available. Production ceased in week 28 before the well was deepened. Monitoring was off line for weeks 29 to 30 and only two events were detected between weeks 31 and 36.

We recorded over 3200 events, average rate 20 events per day over the first 23 weeks. Signals were impulsive and contained significant seismic energy from 10 to over 1500 Hz (**Fig. 6**). Slight anisotropy was observed, horizontally-polarized S waves usually arriving early. Reflections were occasionally observed but were not needed to locate microearthquakes because data from the two geophones in well GT8 constrained depths well. Three shots were recorded for calibration purposes.

### Calibration and Location Methods

Deployments consisted of three or fewer downhole stations, which required us to use a combination of P- and S-wave arrival times and P-wave hodogram azimuths to obtain locations. Arrival times were determined manually. Eigenvector analysis<sup>38</sup> was used to compute hodogram azimuths using the first half-cycle of the horizontal-component P wave. These data gave the propagation azimuth of the P wave, used to constrain the event location.

Calibration of the field site consisted of estimating seismic velocities, station time corrections and azimuthal

geophone orientations. Depths to major geological interfaces were taken from well log data, most often resistivity. All sites were well approximated by horizontally layered models. Initial P-wave velocity was taken from well logs and perforation shot data. S-to-P velocity ratios could also be obtained from perforation shots, but were unreliable because perforation shot records contained poor S waves. Perforation shot hodograms gave initial estimates of geophone orientation.

The velocity and orientation estimates were refined using a joint-hypocenter-velocity inversion, performed using a subset of microearthquakes and shots with high-quality arrival-time and hodogram data. The inversion adjusted unknown velocities, station time corrections, geophone orientations and event locations to fit the arrival-time and hodogram data in a least-squares sense. Units were scaled so timing and angular data were of similar magnitude. Data were weighted by estimates of uncertainty. The parameter separation technique<sup>39</sup> was used so an unlimited number of events could be included. Once a site was calibrated, the remaining event locations could be calculated using standard techniques, employing similar scaling and weighting as above.

## Results

**Austin Chalk.** Initial attempts at locating Austin chalk microearthquakes using hodogram inclinations to constrain depths fared poorly (**Fig. 7**). Events fell well beneath the producing zone, in the more ductile, Eagleford shale. Because the results were so unrealistic, we decided to include reflected phases in the analysis.

Calibration was performed using 90 high-quality events containing two P and two S arrivals and at least one reflected arrival recorded by the two-geophone array during stimulation of the Matcek 1. Results gave a P velocity of 4.71 km/s for the Austin chalk, matching the sonic-log value from a well near Cook's Point. S velocity was 2.38 km/s. The S velocity in the Eagleford shale, beneath the Austin chalk, was constrained by the reflected phase to 1.80 km/s.

Depths of the 90, high-quality microearthquakes were constrained very well by the reflection data, (**Fig. 8**). Most events fell within 20 m of the base of the Austin chalk. We also located Cook's Point events that had all three P, S and reflected phases using the velocities obtained above. Depths were not as well constrained, but still clustered around the base of the Austin chalk.

Given the narrow depth range of the high-quality events, we fixed event depth to the middle of the production interval near the base of the Austin chalk.

This allowed the location of over 240 Matcek-1 stimulation events, defining a linear trend parallel to the expected fracture trend in the Giddings (**Fig. 9**). The most distant events were over 700 m from the Matcek-3 geophone. The entire wing of the stimulation was visible, although the density of locatable events decreased near the injection point. The seismic zone was less than 30 m wide over much of its length.

For the single-station experiment at Cook's Point, all locations were based on P and S (vertically polarized) arrival times and a hodogram azimuth. P waves strong enough to provide high-quality azimuths occurred for only 96 events. We obtained two groups of locations, symmetrical about the station position, because of the ambiguity in hodogram direction. The most likely group aligned with the stimulation well in the direction expected from regional geology (**Fig. 9**). The most distant locatable events were just over 400 m from the monitor station. Thus, we saw only a portion of one wing of the stimulation. The width of the seismic zone was 150 m over most of the observable length. The width was constrained well by P and S arrival times and was affected little by hodogram error.

**Clinton Co.** We calibrated the site using events with three P and three S arrival times, and at least two hodogram azimuths. Setting a layer boundary at the top of the High Bridge (344 m), the hypocenter-velocity inversion gave P velocities of 6.04 and 6.37 km/s and S velocities of 2.93 and 2.95 km/s. Geophone orientations swung as much as 5° from the initial, perforation-shot estimates. The refined geophone orientations were important in aligning locations of events collected before and after deployment of the third geophone. After calibration, we located over 1700 events (**Fig. 10**). Three fracture planes strike N65°E and dip 15° to 20° to the NW or to the SE. The deepest fracture (group C in **Fig. 10**) was difficult to see, but stood out because of its unique, S-nodal (large P, small S) waveforms on the upper GT8 geophone. This plane contained over 200 events forming an elongate planar pattern that intersected the main fracture (group B) along its northern, well-defined edge. Composite focal mechanisms have indicated nearly pure reverse faulting along these fractures<sup>40</sup>.

## Discussion

We collected over 480 and 770 microearthquake events at two Austin chalk sites in the Giddings field, 20% and 31% could be located, respectively. In Clinton Co. we collected over 3200 events, locating 53%. We were encouraged by such successful studies, given the restriction of deploying geophones only in existing wells.

In the Austin chalk, production tubing had to be pulled from wells prior to monitoring. Geophone tools that can be deployed in production tubing or in the annulus will cut this expense from future studies.

Because hodogram inclinations could not be relied on (**Fig. 7**), locating Austin chalk events depended on the use of reflected phases to constrain depths (**Figs. 4, 8**). However, high-quality reflections were present in a minority of events. In Clinton Co. we placed two geophones in one well, 180 m apart, providing depth control for nearly all events.

**Austin Chalk.** If Austin chalk shear-slip events resulted from elevated pore pressure during hydraulic stimulation, the seismic zone should be comparable to the region of the reservoir that was subject to imbibition, or the replacement of hydrocarbons in microcracks with water by capillary action.

Both Austin chalk seismic zones were similarly oriented, parallel to the trend of the regional folding responsible for the reservoir fracture system. However, the Cook's Point seismic zone was five times wider than the Matcek zone. Perhaps a more dense fracture network enabled stimulation over a wide zone at Cook's point, while more competent rock caused the stimulation to drive a single fracture over a long distance at the Matcek site. Production records show a large increase in oil rate from the Cook's Point well immediately following stimulation, but little increase from the Matcek well (**Fig. 11**). The production records suggest that the microseismic patterns are directly related to the effectiveness of the stimulation.

The microearthquake locations fell into a narrow depth interval during the Matcek stimulation (**Fig. 8**). Reservoir engineers predicted containment of the stimulation between a thin, ductile, volcanic ash layer within the Austin chalk and the Eagleford shale. Microearthquake locations supported the containment prediction at the Matcek site.

**Clinton Co.** Clinton Co. microearthquakes defined three, low-angle, reverse slip, fracture zones (**Fig. 10**). Seismic activity was clearly related to the production of over 1300 m<sup>3</sup> (8100 bbl) of oil from well HT1 (**Fig. 5**). However, the seismically active fractures lie above and below the HT1 production interval and intersect or can be extrapolated to old production intervals in wells GT1, GT2 and GT4. In the nine months preceding monitoring, 725 m<sup>3</sup> (4600 bbl) of oil was extracted from these three wells. During the sixth month of monitoring, well GT10 was drilled to the main mapped fracture (Group B in **Fig. 10**) where it produced brine. Well HT1 was subsequently deepened, encountering brine where it intersected the same fracture further updip. This leads us to believe the

microearthquakes defined previously drained, oil-bearing fractures that subsequently recovered to hydrostatic pressure via brine invasion, presumably resulting from an active, but poorly connected water drive<sup>40</sup>.

The observed seismic behavior is consistent with poroelastic models that predict slight increases in horizontal-compressive stress above and below draining volumes<sup>31</sup>. Pressure re-equilibration via denser brine replacing produced oil along the active faults should also weakly promote the observed seismic failure. We estimate the additional stress provided by these two mechanisms that act in directions parallel to the already horizontal-compressive, background state of stress as only 0.02 MPa, implying the fractures were already critically stressed for shear failure<sup>40</sup>.

Storage capacity computed for the most seismically active fracture, based on mapped surface area and well-log porosity estimates, implies that total oil production represents about 20% of the pore volume of the fracture<sup>40</sup>.

The presence of low-angle, oil-bearing fractures has implications for field development. Drilling horizontal or deviated wells should not increase the probability of intersecting productive fractures. Dip meter and formation micro-scanning logs may be very useful in determining orientations of low-angle, productive fractures and thereby aid in more effective placement of offset wells. Interwell correlation and mapping of the conductive fractures will allow better planning in plug-and-abandonment operations so as to avoid premature contamination of pay zones with water. Pressure maintenance operations could also be attempted once the conductive fracture zones between wells have been mapped.

## Conclusions

1. Over 480 and 770 stimulation-induced microearthquakes were recorded at two sites in the Austin chalk, Giddings field, Texas and over 3200 production-induced microearthquakes were recorded at Clinton County, Kentucky, deploying geophones in existing boreholes.

2. Hodogram-inclination data caused Austin chalk events to locate out of zone, leading to the use of reflected phases for depth control. In Clinton County, dual geophone deployment in a single well constrained event depths successfully.

3. Combining shot and well log data with a joint hypocenter-velocity inversion allowed us to calibrate seismic velocities and downhole geophone orientations and to calculate accurate microearthquake locations. Of those collected, 20% and 31% of Austin chalk and 53% of Clinton County microearthquakes could be located.

4. At two Austin chalk sites, microearthquake patterns indicated different stimulation-zone widths; the wider zone yielded higher post-stimulation production. Reflected phases constrained microearthquake depths which fell within the stimulated zone of the Austin chalk.

5. At Clinton County, microearthquakes defined high-porosity, low-angle, reverse-slip fracture zones that previously produced oil and have since recovered to hydrostatic pressure via brine invasion. No seismicity intersected the currently producing interval. These observations are consistent with stress changes associated with poroelastic effects<sup>31</sup> and the mass exchange of brine replacing produced oil<sup>40</sup>.

## Acknowledgments

We thank Michael Fehler, James Albright, Robert Hanold, Jay Bertram and Nick Valenti for their efforts in initiating these projects. Dave Anderson, Rick Flora, Joel Duran, Richard Maestas, Leigh House, Grady Rhodes and Rod Flores assisted with data acquisition. Additional thanks to Butch Humphries, Cab Craig, Chris Ruisaard and employees of BJ Services, Bryan and Magnum Wireline, Giddings, for field support in the Austin chalk and to Lynn Wagoner of the Ohio Kentucky Oil Corp for field support in Clinton County. Reviews by Don Dreesen and Lee Steck and an anonymous referee helped to improve the manuscript. These projects were supported by the U.S. Department of Energy, Natural Gas and Oil Recovery Partnership.

## References

1. Snaman, D.K., Hunter, R.J. and Wood, M.D., "Tiltmeter mapping of fractures in granitic rock at Wawona, Yosemite National Park, California," *EOS Trans, Am. Geophys. Union*, (1993) **74**, 582.
2. Branagan, P.T., Warpinski, N.R., Engler, B.P. and Wilmer, R., "Measuring the hydraulic fracture-induced deformation of reservoir and adjacent rocks employing a deeply buried inclinometer array: GRI/DOE Multi-Site Project," paper SPE 36451, presented at the 1996 SPE Annual Technical Conference and Exhibition, Denver, October 6-9.
3. Barton, C.A., Zoback, M.D. and Moos, D., "Fluid flow along potentially active faults in crystalline rock," *Geology*, (1995) **23**, 683.
4. Stewart, R.R., Turpening, R.M. and Toksoz, M.N., "Study of a subsurface fracture zone by vertical seismic profiling," *Geophys. Res. Lett.*, (1981) **8**, 1132.
5. Turpening, R.M. and Blackway, C., "Differential vertical seismic profiling: The hydrofrac," in Balch, A., and Lee, M., Eds., *Vertical Seismic Profiling*, Internat. Human Res. Develop Corp., (1984).
6. Niitsuma, H. and Saito, H., "Evaluation of the three-dimensional configuration of a subsurface artificial fracture by the triaxial shear shadow method," *Geophysics*, (1991)

- 56, 2118.
7. Meadows, M.A. and Winterstein, D.F., "Seismic detection of a hydraulic fracture from shear-wave VSP data at Lost Hills Field, California," *Geophysics*, (1994) **59**, 11.
  8. Warpinski, N.R. and Teufel, L.W. "Influence of geologic discontinuities on hydraulic fracture propagation," *JPT*, (1987) **39**, 209.
  9. Fast, R.E., Murer, A.S. and Timmer, R.S., "Description and analysis of cored hydraulic fractures: Lost Hills Field, Kern County, California," *SPE Production and Facilities*, (1994) **9**, 107.
  10. Mueller, M.C., "Using shear waves to predict lateral variability in vertical fracture intensity," *The Leading Edge*, (1992) **11**, 29.
  11. Pearson, C., "The relationship between microseismicity and high pore pressure during hydraulic stimulation experiments in low permeability granite rocks," *J. Geophys. Res.*, (1981) **86**, 7855.
  12. Albright, J.N. and Pearson, C.F., "Acoustic emissions as a tool for hydraulic fracture location: experience at Fenton Hill Hot Dry Rock site," *SPE Journal* (1982) **22**, 523.
  13. House, L. S., "Locating microearthquakes induced by hydraulic fracturing in crystalline rock," *Geophys. Res. Lett.*, (1987) **14**, 919.
  14. Batchelor, A., Baria, S.R. and Hearn, K., "Monitoring the effects of hydraulic stimulation by microseismic event location, a case study," paper SPE 12109, presented at the 1983 SPE Annual Technical Conference and Exhibition, San Francisco, October 5-8.
  15. Baria, R. and Green, A., "Seismicity induced during a viscous stimulation at the Camborne School of Mines Hot Dry Rock geothermal Energy project in Cornwall, England," *Proc. Progress in Acoustic Emission*, (1986) **3**, 407.
  16. Niitsuma, H., Chubachi, N. and Takanohashi, M., "Acoustic emission analysis of a geothermal reservoir and its application to reservoir control," *Geothermics*, (1987) **16**, 47.
  17. Cornet, F.H., "Projet Mayet de Montagne, Etude in situ de la percolation forcee d'eau an milieu granitique" (in French), *Final Report, IGP*, (Sept. 1988).
  18. Block, L., Fehler, M.C., Cheng, C.H. and Phillips, W.S., "Seismic imaging using microearthquakes induced by hydraulic fracturing," *Geophysics*, (1994) **59**, 102.
  19. Fehler, M.C., House, L.S. and Kaieda, H., "Determining planes along which earthquakes occur: method and application to earthquakes accompanying hydraulic fracturing," *J. Geophys. Res.*, (1987) **92**, 9407.
  20. Roff, A., Phillips, W.S. and Brown, D.W., "Joint structures determined by clustering microearthquakes using waveform amplitude ratios," *Int. J. Rock Mech. Min. Sci. Geomech. Abstr.*, (1996) **33**, 627.
  21. Phillips, W.S., House, L.S. and Fehler, M.C., "Detailed joint structure in a geothermal reservoir from studies of induced microearthquake clusters," *J. Geophys. Res.*, (1997) **102**, 11745.
  22. Dobecki, T. L., "Hydraulic fracture orientation by use of passive borehole seismics," paper SPE 12110, presented at the 1983 SPE Annual Technical Conference and Exhibition, San Francisco, October 5-8.
  23. Sarda, J.-P., Perreau, P.J. and Deflandre, J.-P., "Acoustic emission interpretation for estimating hydraulic fracture extent," paper SPE 17723, presented at the 1988 SPE Gas Technology Symposium, Dallas, June 13-15.
  24. Fix, J.E., Adair, R.G., Fisher, T., Mahrer, K., Mulcahy, C., Myers, B., Swanson, J., and Woerpel, J.C., "Development of microseismic methods to determine hydraulic fracture dimensions," *Gas Res. Inst., Tech. Rep.* (1989) **No. 89-0116**.
  25. Vinegar, H. J., Wills, P.B., DeMartini, D.C., Shylapobersky, J., Deeg, W.F., Adair, R.G., Woerpel, J.C., Fix, J.E. and Sorrells, G.G., "Active and passive seismic imaging of a hydraulic fracture in diatomite," paper SPE 22756, presented at the 1991 SPE Annual Technical Conference and Exhibition, Dallas, Texas, October 6-9.
  26. Stewart, L., Cassell, B.R. and Bol, G.M., "Acoustic-emission monitoring during hydraulic fracturing," *SPE Formation Evaluation* (1992) **7**, 139.
  27. Keck, R.G. and Withers, R.J., "A field demonstration of hydraulic fracturing for solid waste injection with real-time passive seismic monitoring," paper SPE 28495, presented at the 1994 SPE Annual Technical Conference and Exhibition, New Orleans, September 25-28.
  28. Zhu, X., Gibson, J., Ravindran, N., Zinno, R., Sixta, D., "Seismic imaging of hydraulic fractures in Carthage tight sands: A pilot study," *The Leading Edge*, (1996) **15**, 218-224.
  29. Warpinski, N.R., Engler, B.P., Young, C.J., Peterson, R., Branagan, P.T. and Fix, J.E., "Microseismic mapping of hydraulic fractures using multi-level wireline receivers", paper SPE 30507, presented at the 1995 SPE Annual Technical Conference and Exhibition, Dallas, October 23-25.
  30. Pennington, W.D., Davis, S.D., Carlson, S.M., Dupree, J. and Ewing, T.E., "The evolution of seismic barriers and asperities caused by the depressuring of fault planes in oil and gas fields of South Texas," *Bull. Seism. Soc. Am.*, (1986) **76**, 939.
  31. Segall, P., "Earthquakes triggered by fluid extraction," *Geology*, (1989) **17**, 942.
  32. Grasso, J.R., and Wittlinger, G., "Ten years of seismic monitoring over a gas field," *Bull. Seism. Soc. Am.*, (1990) **80**, 450.
  33. Doser, D.I., Baker, M.R., and Mason, D.B., "Seismicity in the War-Wink gas field, Delaware Basin, Texas, and its relationship to petroleum production," *Bull. Seism. Soc. Am.*, (1991) **81**, 971.
  34. Hamilton-Smith, T., Nuttall, B.C., Gooding, P.J., Walker, D., and Drahovzal, J.A., "High-volume oil discovery in Clinton County, Kentucky," *Kentucky Geological Survey, Series 11, Information Circular 33*, (1990).
  35. Black, D.F.B., "Oil in dolomitized limestone reservoirs in Kentucky," *Proc. 6th Int. Conf. Basement Tectonics*, (1986) **140**.
  36. Rutledge, J.T., Phillips, W.S., Roff, A. Albright, J.N., Hamilton-Smith, T., Jones, S.K. and Kimmich, K.C., "Subsurface fracture mapping using microearthquakes detected during primary oil production, Clinton County,

Kentucky", paper SPE 28384, presented at the 1994 SPE Annual Technical Conference and Exhibition, New Orleans, September 25-28.

37. Lee, W.H.K., "Toolbox for seismic data acquisition, processing and analysis," *IASPEI Software Library*, (1989) 1.
38. Flinn, E.A., "Signal analysis using rectilinearity and direction of particle motion", *Proc. IEEE*, (1965) **53**, 1725.
39. Pavlis, G.L. and Booker, J.R., "The mixed discrete-continuous inverse problem: Application to the simultaneous determination of earthquake hypocenters and velocity structure," *J. Geophys. Res.*, (1980) **85**, 4801.
40. Rutledge, J.T., Phillips, W.S. and Schuessler, B.K., "Reservoir characterization using oil-production induced microseismicity, Clinton County, Kentucky, " *Tectonophysics*, in press.

---

**Scott Phillips** is a technical staff member at Los Alamos National Laboratory. When this work was performed, he was an officer and Project Geophysicist with Nambe Geophysical, Inc. His research interests include test-ban treaty verification, induced seismicity, tomography and local earthquake studies. He holds a Ph.D. from M.I.T. and a B.A. from the University of California, Berkeley, both in geophysics.

**James T. Rutledge** is a Senior Geophysicist at Nambe Geophysical, Inc. and has been working as a consulting geophysicist at Los Alamos National Laboratory since 1984. His research interests include borehole seismology, wave propagation in layered media and induced reservoir microseismicity. He holds a B.S. degree in geology from Penn State and a M.S. in geophysics from the University of Arizona.

**Thomas D. Fairbanks** is a founding partner of Nambe Geophysical, Inc. Before that he was a consultant to Los Alamos National Laboratory in borehole seismic instrumentation. Before boreholes, he worked on the seafloor as a staff member in the College of Oceanography at Oregon State University. He holds a B.S. in electrical and computer

engineering from Oregon State University.

**Thomas L. Gardner** is a consulting reservoir engineer for Ryder Scott Company Petroleum Engineers in Houston. He was previously with Exxon Co. U.S.A., ARCO Alaska, Inc., and Sun E&P Co. and has a B.S. in petroleum engineering and an M.B.A., both from Texas A&M University.

**Michael E. Miller** is a senior exploration geologist with Exxon Exploration Company in Houston and is currently working the deep water Gulf of Mexico. He holds a B.A. from Thiel College in western Pennsylvania and an M.S. from Texas A&M University in geology. He has been with Exxon since 1979.

**Barbra Schuessler Maher** is currently working on her Ph.D. at Colorado School of Mines with the Reservoir Characterization Project. She obtained her M.S. from University of Arizona in geophysics and her B.S. in physics from Austin Peay State University. She also worked with Los Alamos National Laboratory studying induced microseismicity.

---

#### Figure Captions

1. Map showing two monitoring sites in the Giddings field, Texas.
2. Map showing the monitoring site in Clinton County, Kentucky.
3. Event histogram and well-head pressure during hydraulic stimulation, well CPU2-2, Giddings field, Texas.
4. Vertical, radial, transverse ground motion velocity and radial-vertical product traces for a CPU2-2 stimulation event, Giddings field, Texas (top) and P, Sv and noise spectra (bottom).
5. Cumulative production, well HT1 and cumulative number of seismic events, Clinton County, Kentucky.
6. Vertical, upper and lower (unrotated) components of ground motion velocity, Clinton County, Kentucky (top) and P and noise spectra (bottom).
7. Cross-section along fracture trend showing locations calculated using hodogram inclinations, Matcek 1 stimulation, Giddings field, Texas. Triangles are borehole geophones and a circle marks the injection interval.
8. East-west cross-section showing locations calculated using reflected phases, Matcek 1 stimulation, Giddings field, Texas. Triangles are borehole geophones and a circle marks the injection interval.
9. Map views of locations for CPU2-2 and Matcek 1 stimulations after constraining locations to the injection depth, Giddings field, Texas.

10. Map and cross-section (C-D) views showing event locations associated with production in well HT1, Clinton County, Kentucky.

11. Pre- and post-stimulation production rates, CPU2-2 and Matcek 1 wells, Giddings field, Texas.

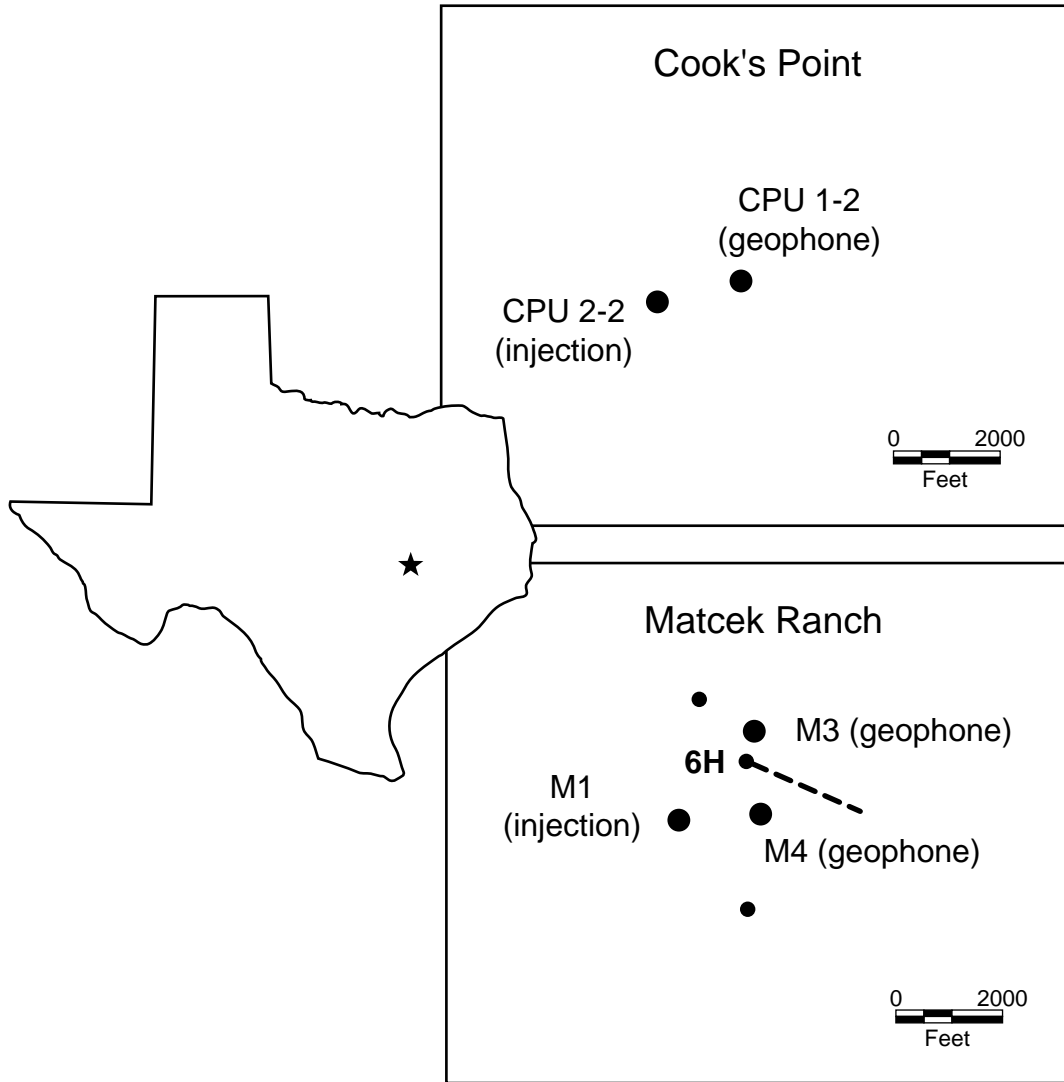


Figure 1

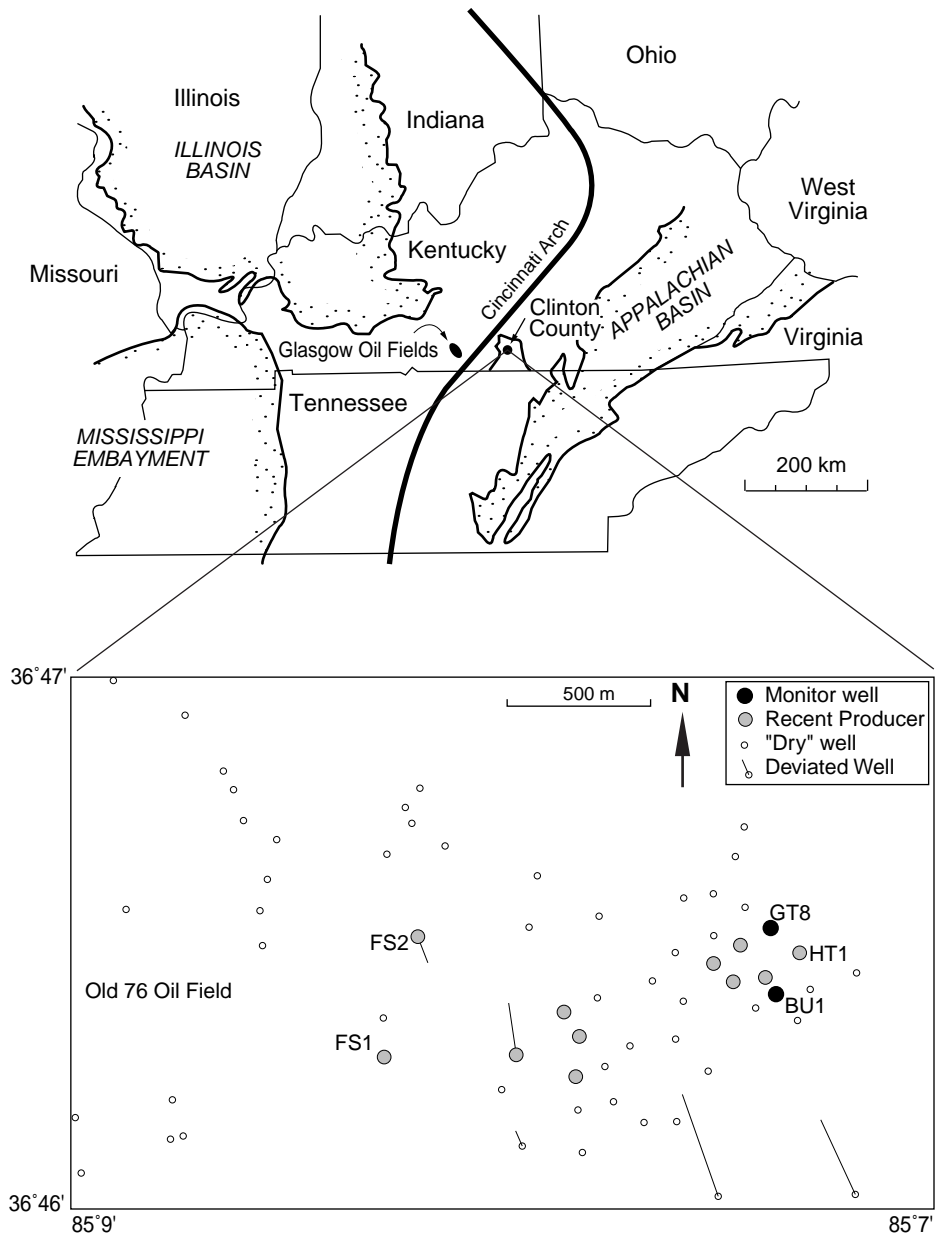


Figure 2

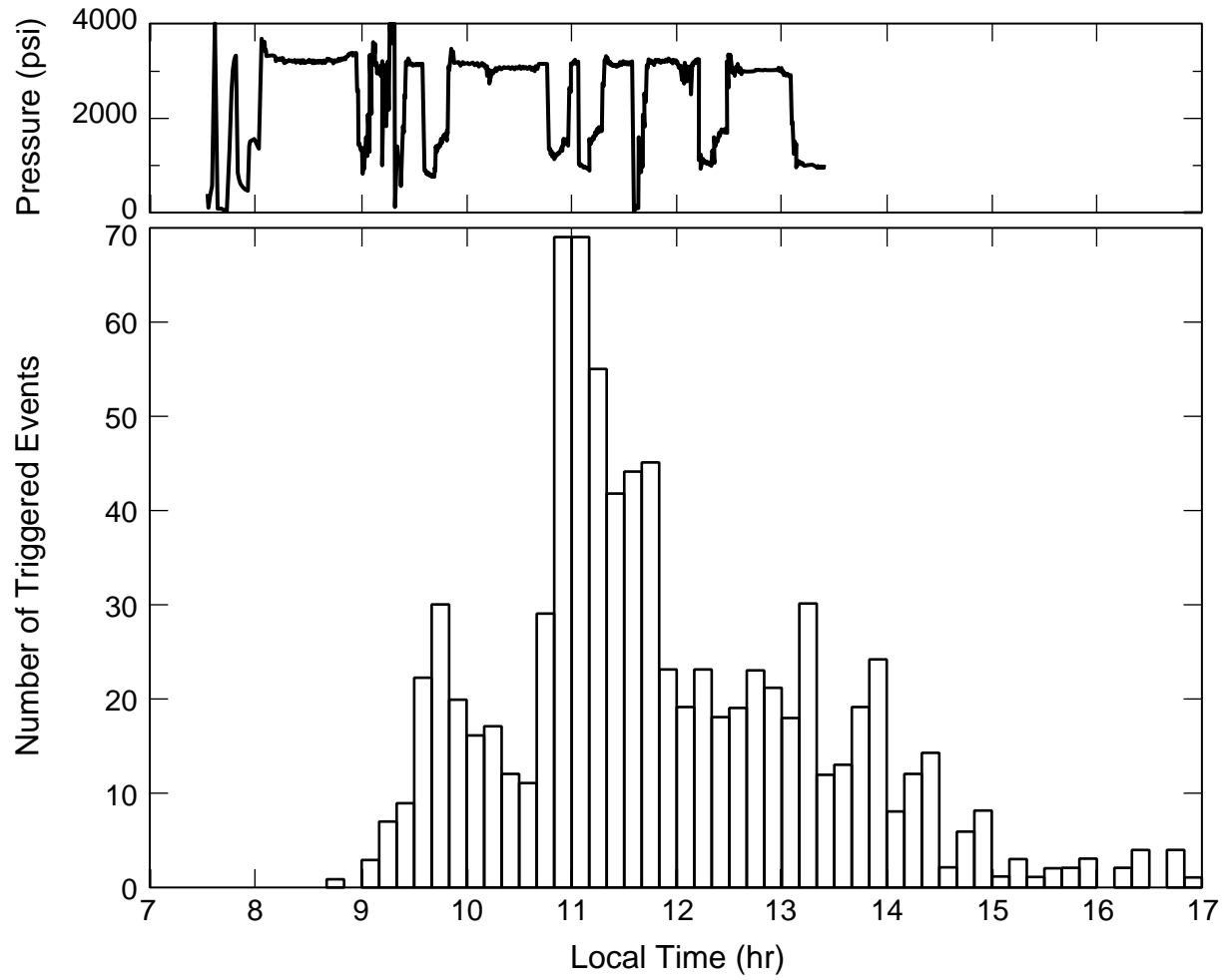


Figure 3

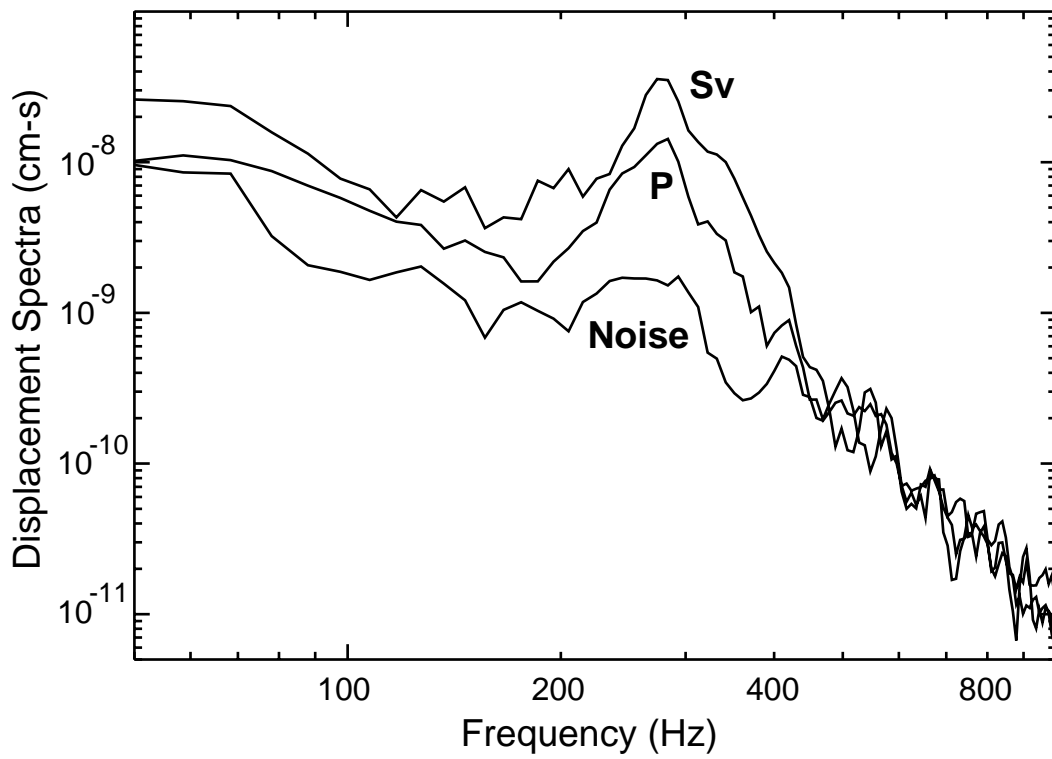
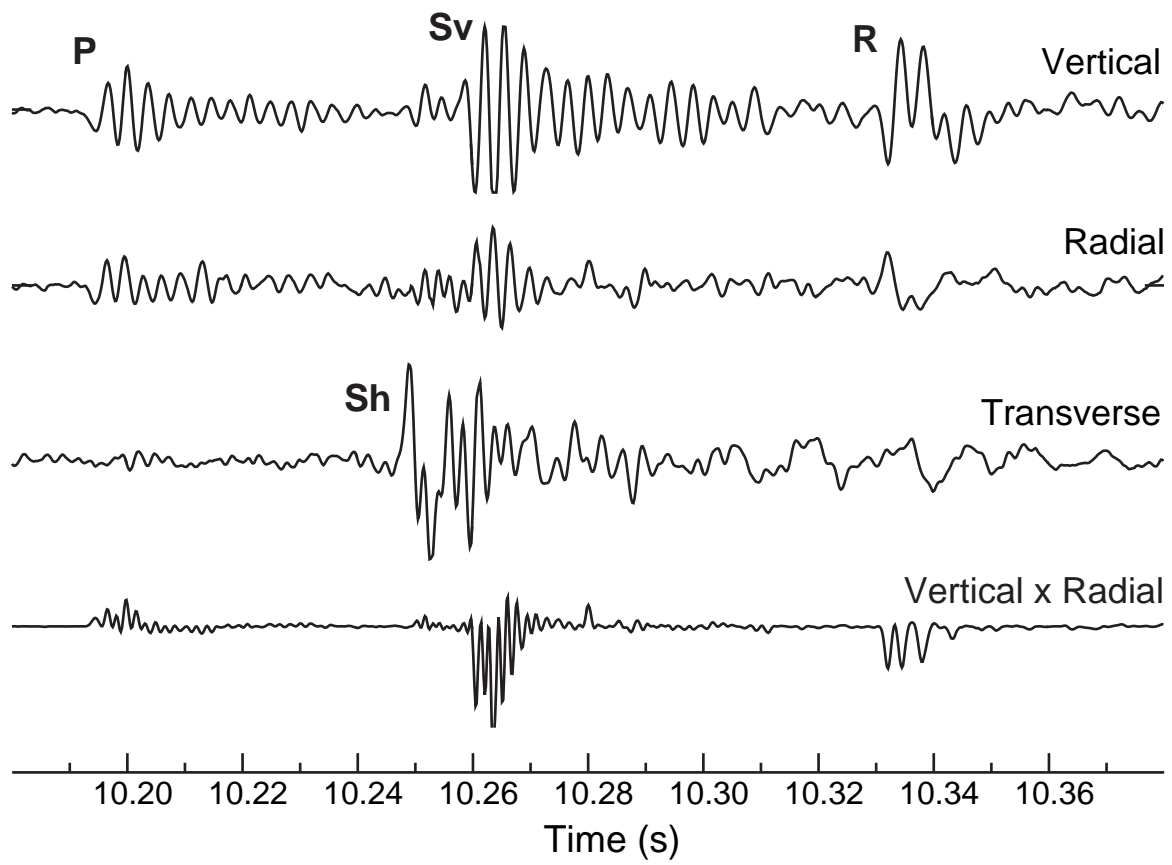


Figure 4

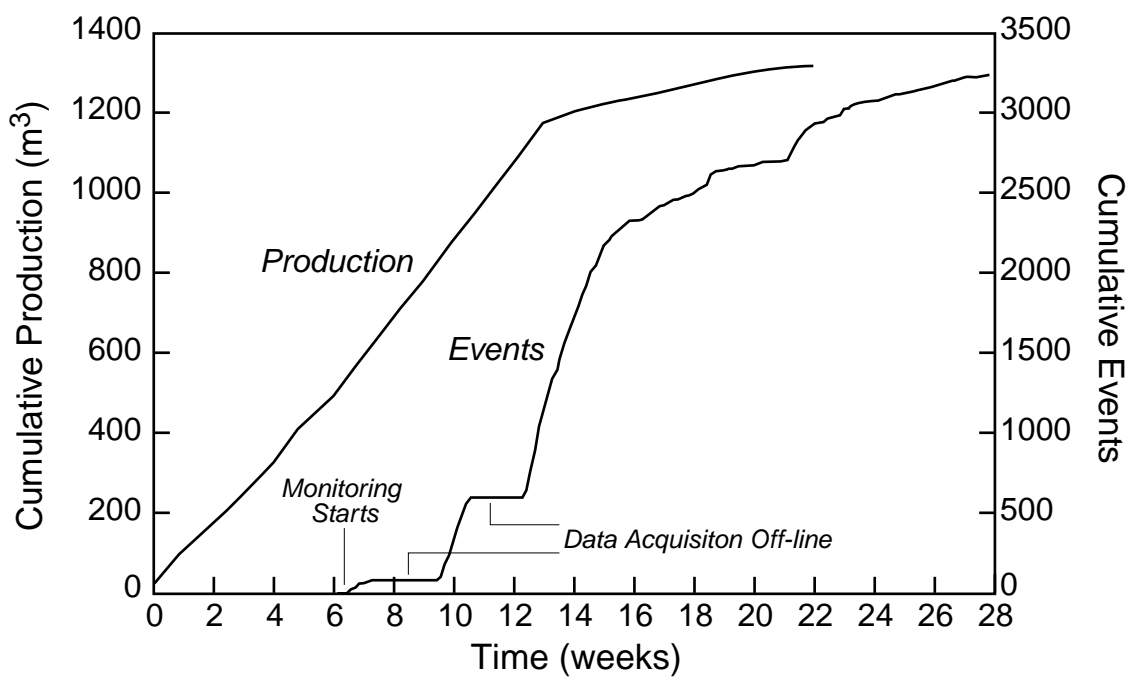


Figure 5

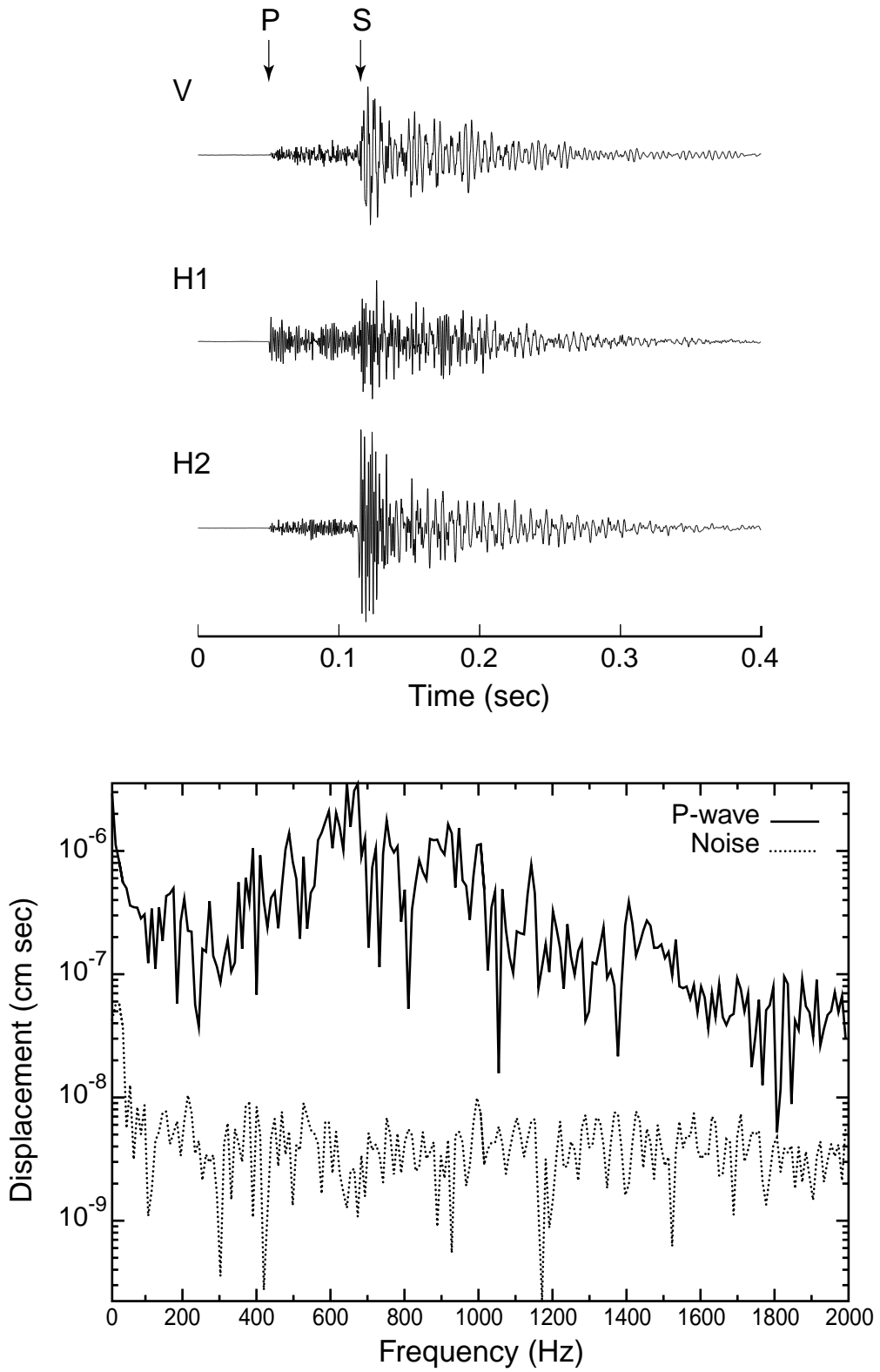


Figure 6

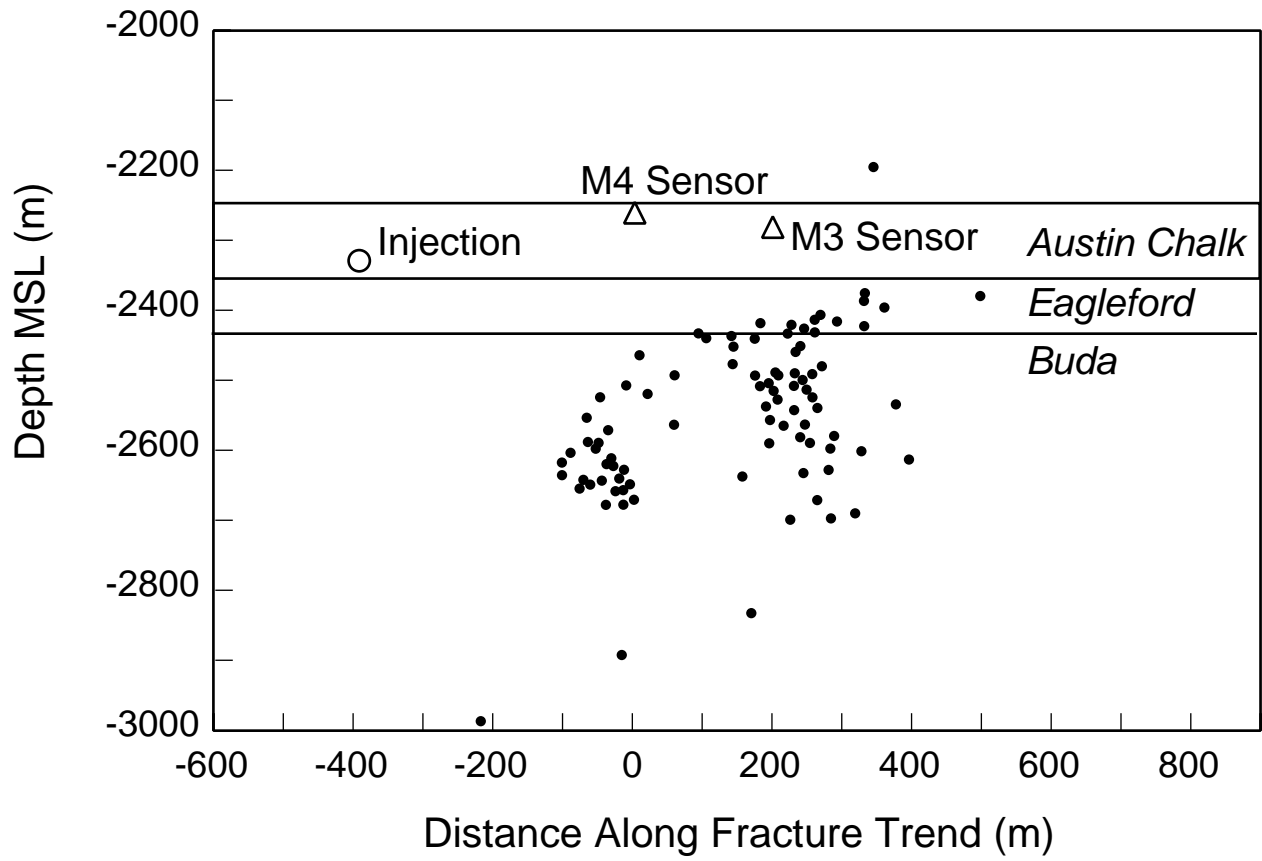


Figure 7

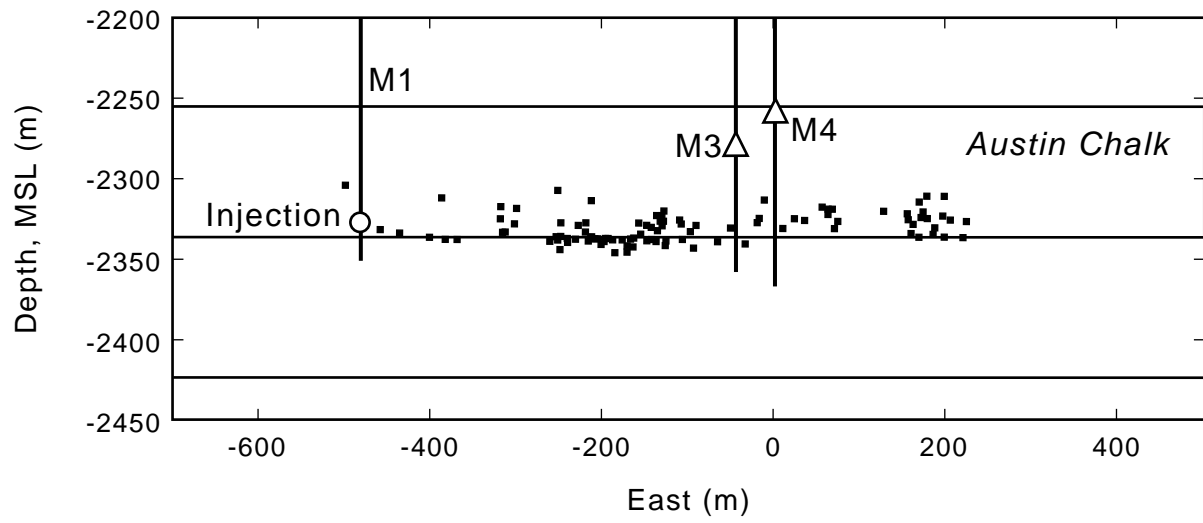


Figure 8

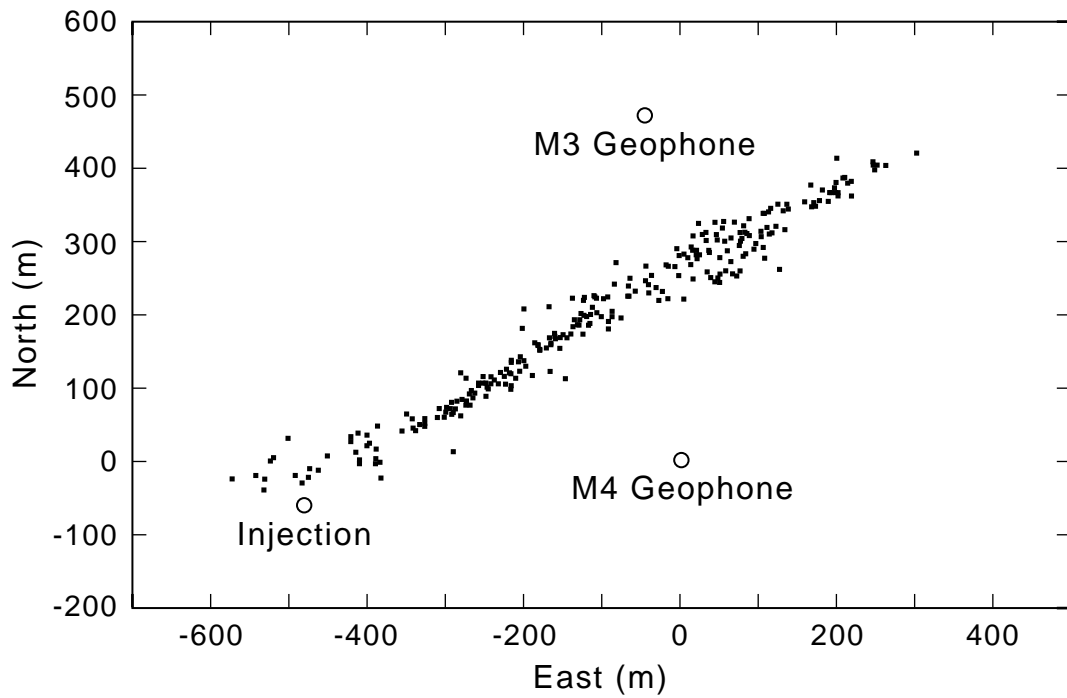
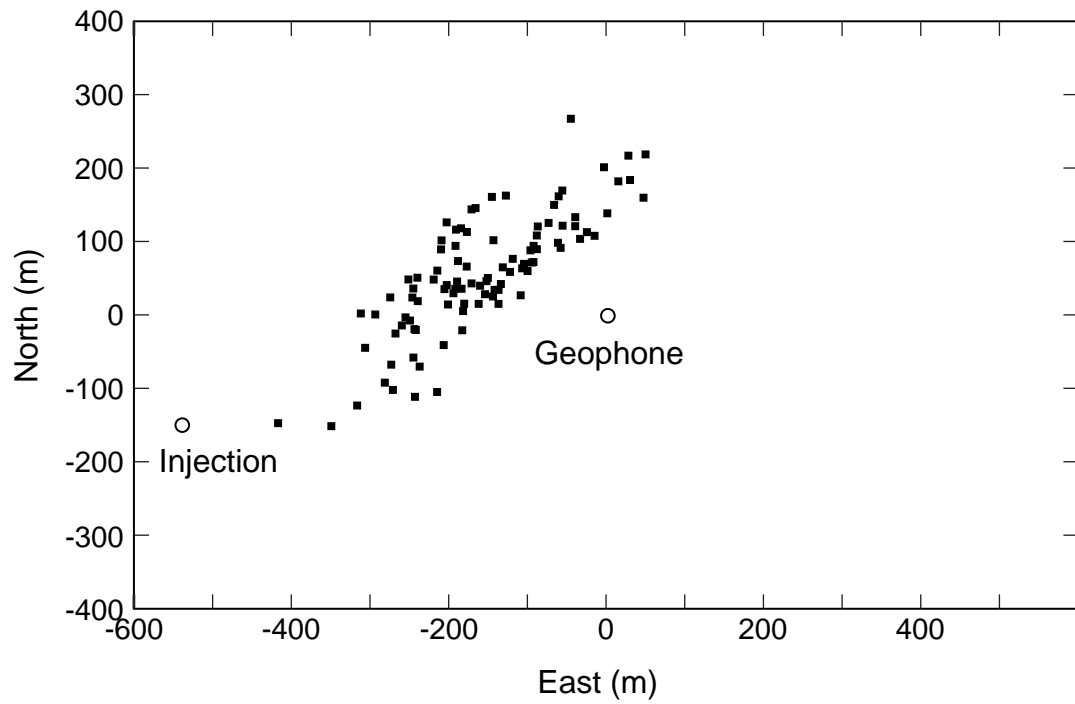


Figure 9

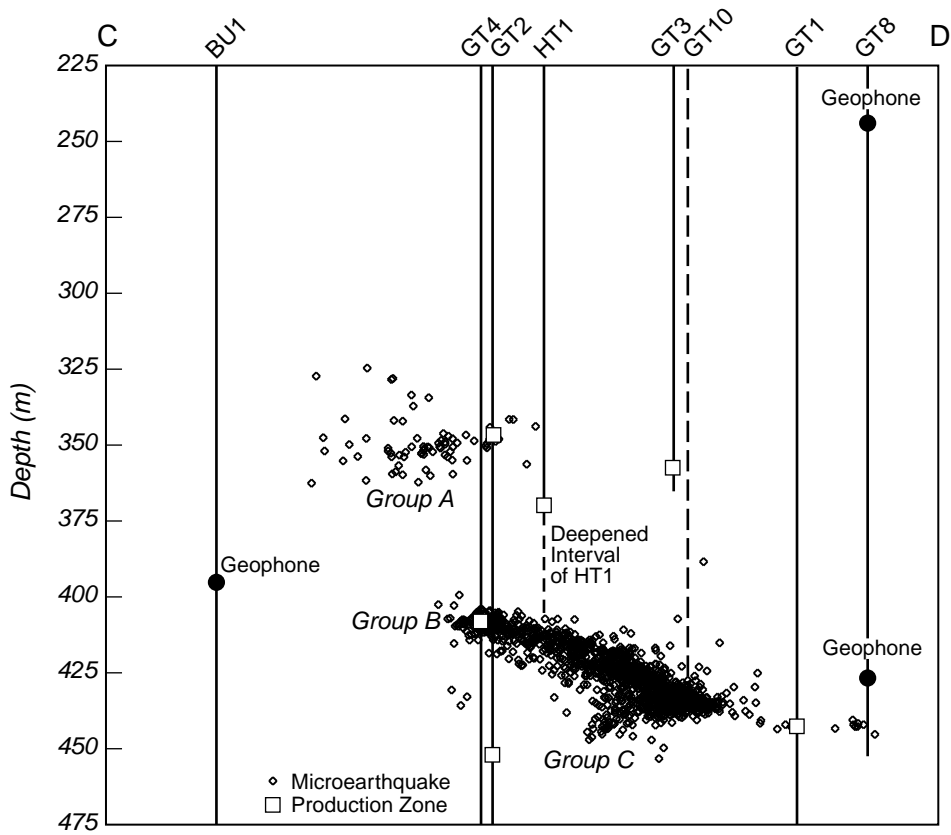
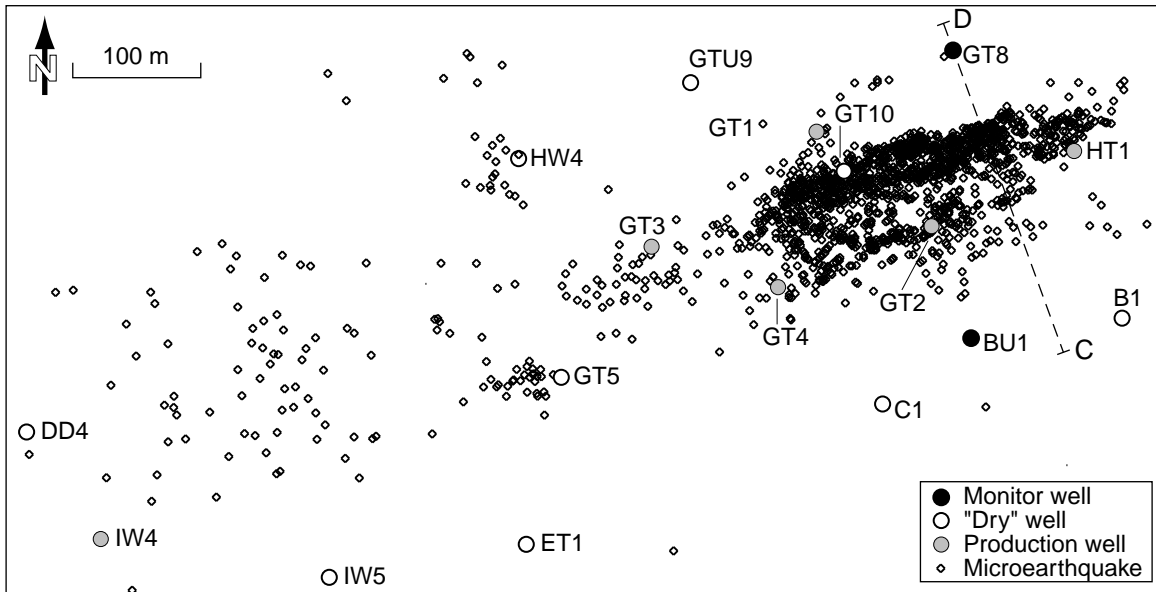


Figure 10

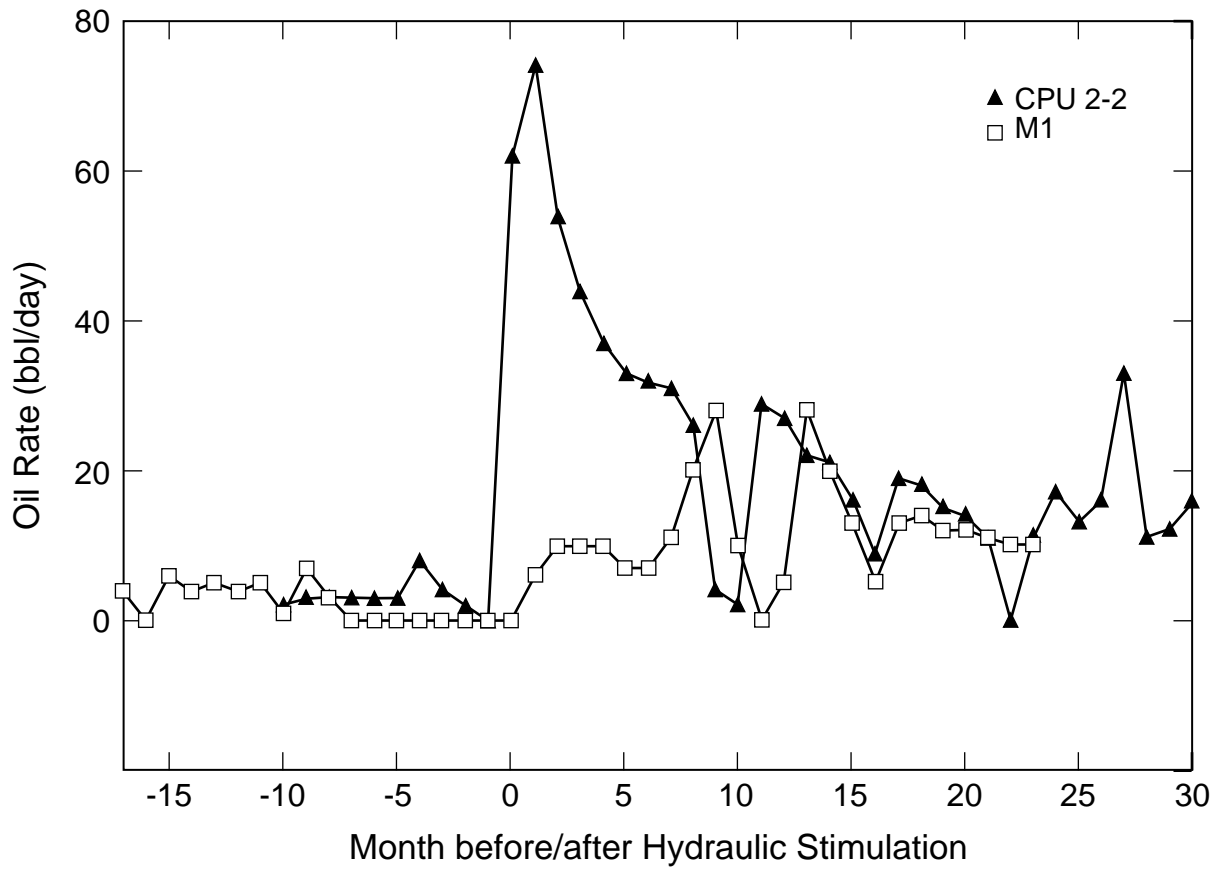


Figure 11